COMBINING OPTICAL AND RADAR SATELLITE IMAGE DATA FOR SURVEILLANCE OF COASTAL WATERS*

J.J. van der Sanden[1], P.W. Vachon[1] and J.F.R. Gower[2]

[1]Canada Centre for Remote Sensing (CCRS)
Ottawa, Ontario, Canada
sanden@ccrs.nrcan.gc.ca

[2]Institute of Ocean Sciences (IOS)
Sidney, British Columbia, Canada
gowerj@dfo-mpo.gc.ca

ABSTRACT

In this paper, we present preliminary results of a study concerning the joint application of optical and radar satellite image data for the mapping / monitoring of coastal waters. The image data studied were acquired during the summer of 1999 by the RADARSAT SAR system and the NOAA AVHRR scanner. Our area of interest is located at Canada's West Coast and includes the waters that surround the Queen Charlottes and Vancouver Island. The findings illustrate the limitations that clouds and wind speed create for the applicability of optical and radar data, respectively. The importance of slicks as tracers of coastal features in SAR images is demonstrated and agreement in the patterns present in thermal AVHRR and SAR data is observed.

1.0 INTRODUCTION

The dynamics of coastal waters are driven by gradients in physical properties such as temperature, salinity, sea surface topography, and suspended particles. In combination, these physical parameters affect all biological processes in the coastal zone. Consequently, information on these parameters is of interest to parties involved in the management and utilisation of coastal resources. As an example, information on currents, waves, and sediment load is relevant to the study of coastal evolution and to the development of plans for coastal protection. Similarly, information on currents and sea surface temperature is of value to stakeholders in the fisheries industry. Several of these important parameters can be observed by means of remote sensing. Measurements from different sensors may reveal different phenomena or may show the same phenomena in a different way. In this paper, we report on the early results of a project that addresses the information content and the applications potential of measurements from a combination of optical and radar satellite systems.

Optical and radar satellite systems operate in different parts of the electromagnetic spectrum. The operating spectrum of the currently available optical satellites extends from approximately 0.4 to 14 μm and includes visible, near-, mid-, and thermal IR wavelengths (Lillesand and Kiefer, 1987). The microwave portion of the electromagnetic spectrum ranges

* Presented at the Sixth International Conference on Remote Sensing for Marine and Coastal Environments, Charleston, South Carolina, 1-3 May 2000.

from 0.8 to 100 cm. Yet, the operating wavelengths of currently orbiting civilian radar satellites are restricted to the so-called C-band - that is - the range from 5.61 to 5.71 cm. Images acquired by optical satellites typically contain information relating to the chemical or thermal properties of observed water bodies. On the other hand, the information content of radar images is governed by the observed water surface roughness. Differences in sensitivity to water properties explain why optical and radar satellites make complementary tools for coastal surveillance. The advance of satellite systems capable of acquiring optical and radar data in simultaneous fashion (e.g. Envisat, ALOS) paves the way for studies into the techniques for and the pros / cons of the joint application of optical and radar satellite data.

2.0 STUDY AREA

The study area is located at Canada's West Coast and includes the waters surrounding the Queen Charlotte Islands and Vancouver Island (Figure 1). Features of interest in these waters may include surface waves, internal waves, currents, eddies, slicks and atmospheric fronts. The current regime along the west coast of Vancouver Island is of special interest because of its distinct seasonable patterns. A network of operational data buoys covers the area of interest. The wind data collected by these buoys are available to the study by IOS. Earlier remote sensing studies that focus on this particular area include those by Vachon et al. (1992) and Gower (1993,1996).

3.0 IMAGE DATA

The images studied were acquired during the summer of 1999 by the RADARSAT SAR system and the NOAA AVHRR scanner. The SAR images were taken on the dates listed in Table 1 at approximately 7 PM local time (PDT). RADARSAT operated in the ScanSAR Wide Beam mode (C-band, swath 450 km, pixel spacing 50 m by 50 m, incidence angle 20º to 46º). To date, only four RADARSAT scenes have been processed. Processing was done at CCRS using the IOSAT ScanSAR processor and included absolute radiometric calibration. The applied AVHRR data were acquired by either the NOAA 12, 14 or 15 satellite within a window from 24 hours before to 24 hours after the RADARSAT acquisition time. This time-window was adopted to enhance the chances of images with acceptable cloud coverage. Even so, it was found to be impossible to attain suitable AVHRR images for eight out of 18 RADARSAT acquisition dates. The AVHRR data sets were downloaded from the NOAA Satellite Active Archive. Each set comprises five full resolution images (pixel spacing 1 km by 1 km) that correspond to visible (red), near infrared, mid infrared and thermal infrared wavelengths. At the time that this paper was written, no attempt had been made to calibrate the AVHRR data. However, calibration of these data will be pursued in future.

4.0 IMAGE ANALYSIS APPROACH

The image analysis approach adopted consisted of a pre-processing step and a data fusion step. Pre-processing started with the geometrical transformation of both the SAR and the AVHRR images to the UTM WGS 1984 grid. During this process, the pixel spacing of the

images was resampled to 200 m by 200 m. Subsequently, the AVHRR channels 1 (visible) and 2 (near IR) were used to generate a cloud / land mask by means of thresholding. Finally, the six available images (five AVHRR, one SAR) were re-scaled to attain optimum contrast in coastal water areas.

Preliminary visual interpretation of selected AVHRR images showed that the visible and near IR channels contained little information. Hence, it was decided to exclude these channels from the data fusion process. Fusion of the AVHRR and SAR images was achieved by applying two straightforward image-processing techniques, namely principal component analysis (PCA) and Red-Green-Blue (RGB) colour space transformation. PCA was used to consolidate the primary information from the AVHRR channels 3, 4 and 5 to a single image – that is – the first principal component (PC1). The PC1 image contains information on sea surface temperature (SST) because the three input channels are sensitive to the thermal properties of observed water bodies. An RGB transformation was then applied using the SAR image, the PC1 image and a grey channel with digital values set to 127 as input. The result of this RGB transformation is an image product in which the brightness relates to the radar backscatter level, the colour to the sea surface temperature and the colour purity to the digital value of the grey channel. Unfortunately, the fused colour composite images could not be included in this paper. Samples of the component SAR and PC1 images will be shown instead.

5.0 RESULTS AND DISCUSSION

Figures 2a and 2b show subsets of the SAR image for 29 July and the AVHRR derived PC1 image for 30 July, respectively. The area shown is located southwest of Estevan Point, Vancouver Island and covers approximately 154 km by 154 km. The grey tones in the PC1 image are chosen proportional to the SST. Hence, dark (light) tones are indicative of relatively low (high) temperatures. Land surface areas appear white in both image subsets. In Figure 2b, areas covered by clouds are also shown in white.

The SAR image shows wind patterns and slicks of unknown origin that mark the location of the coastal current. Due to the limited spatial resolution, small-scale coastal features like slicks cannot be observed in AVHRR images. Despite the close to 24 hours difference in acquisition time, the patterns in the Figures 2a and 2b are very similar. Comparison of the two figures suggests that the slicks are concentrated in areas with relatively high surface temperatures. The visibility of surface slicks in SAR images is highly dependent on wind speed. This will be discussed in more detail in connection with Figures 3 and 4.

Figure 3 shows two subsets that were taken from a SAR and an AVHRR image acquired on 16 October and 15 October, respectively. Like in Figure 2, the images cover an area of circa 154 km by 154 km. The grey tone scheme of the PC1 image in Figure 3b conforms to the one discussed in relation to Figure 2b.

The SAR image in Figure 3a shows three features of interest, namely an eddy, a train of internal waves, and an atmospheric front. The eddy is clearly visible since its rotational flow is

outlined by naturally-occurring surfactant slicks. Using the knowledge obtained from the SAR image it is possible to also infer the presence of the eddy from the thermal patterns in Figure 3b. The internal waves shown in Figure 3a are not apparent in the AVHRR image. The dark area in the SAR image identifies a smooth sea surface resulting from the presence of an atmospheric front. This front is associated with a local change in wind speeds. To the left of the front, the wind speed is lower than to the right. This may be deduced from the backscatter signature and model results presented in Figure 4. The SAR wind retrieval model applied is described in Vachon and Dobson (2000).

The image subset shown Figure 4a covers the complete ScanSAR Wide Beam swath width and includes most of the area shown in Figure 3a. Again, the locations of the eddy and the atmospheric front have been identified. The horizontal line, about two-thirds from the top of the image, marks the position of the backscatter transect presented in Figure 4b. The superimposed model results (dashed curves) reveal that the wind speeds to the left and right of the front are of the order of 3 and 7 m s^{-1}, respectively. These wind speeds constitute the lower and upper limits for visibility of coastal features including surfactant slicks, eddies, currents and internal waves. At lower wind speeds, such features will go unobserved, as the sea surface is too smooth to generate a significant radar return signal. This is well illustrated in Figure 4b, where it can be seen that the backscatter to the east of the atmospheric front drops to the noise floor. At higher wind speeds, subtle roughness differences, as induced by the features that were discussed, are lost and the sea state, and hence the radar backscatter, are dominated by wind-induced surface waves.

6.0 CONCLUDING REMARKS

Our study as to how to exploit optical and radar remote sensing data for the surveillance of coastal waters is still in its infancy. The available data need to be examined both to a larger extent and in more detail. In future, we plan to evaluate and, if necessary, develop different methods/techniques for data fusion. Moreover, we intend to work with data from other (and future) satellite systems such as SeaWIFS, Envisat and ALOS. The latter two systems offer great potential for our studies because of the capability to acquire coincident optical and radar images.

The results presented in this paper confirm two findings commonly reported in studies that apply either optical or radar data. Namely, that the applicability of optical data is limited by cloud cover and that the applicability of radar data is limited by wind speed. Consequently, it is has proven to be more difficult to obtain a suitable combination of optical and radar data than to obtain acceptable optical or radar data separately. On the other hand, once the information content of both data sources is fully understood and links have been established, it may be feasible to infer certain information from either date set. The success of this approach would represent a good example of the synergy obtained by combining optical and radar remote sensing data.

7.0 REFERENCES

Gower, J.F.R., "Mapping coastal currents with SAR, using naturally-occurring surface slick patterns." In *Proceedings of the Second ERS-1 Symposium; Space at the Service of Our Environment*, Hamburg, pp.415-418, 11-14 October 1993.

Gower, J.F.R., "Coastal current model validation using satellite images of bright blooms." In *Proceedings of the 18th Symposium of the Canadian Remote Sensing Society, Information Tools for Sustainable Development*, Vancouver, pp.229-232, 25-29 March 1996.

Lillesand, T.M. and R.W. Kiefer, *Remote Sensing and Image Interpretation,* John Wiley & Sons, New York, p.721, 1987.

Vachon, P.W., G.A. Borstad, and R.E. Thomson, "Airborne SAR observations of mesoscale ocean features," *Canadian Journal of Remote Sensing,* Vol.18, No.3, pp.152-165, 1992.

Vachon, P.W., and F.W. Dobson, "Wind retrieval from RADARSAT SAR images: Selection of a suitable C-band HH polarization wind retrieval model," in press, *Canadian Journal of Remote Sensing*, 2000.

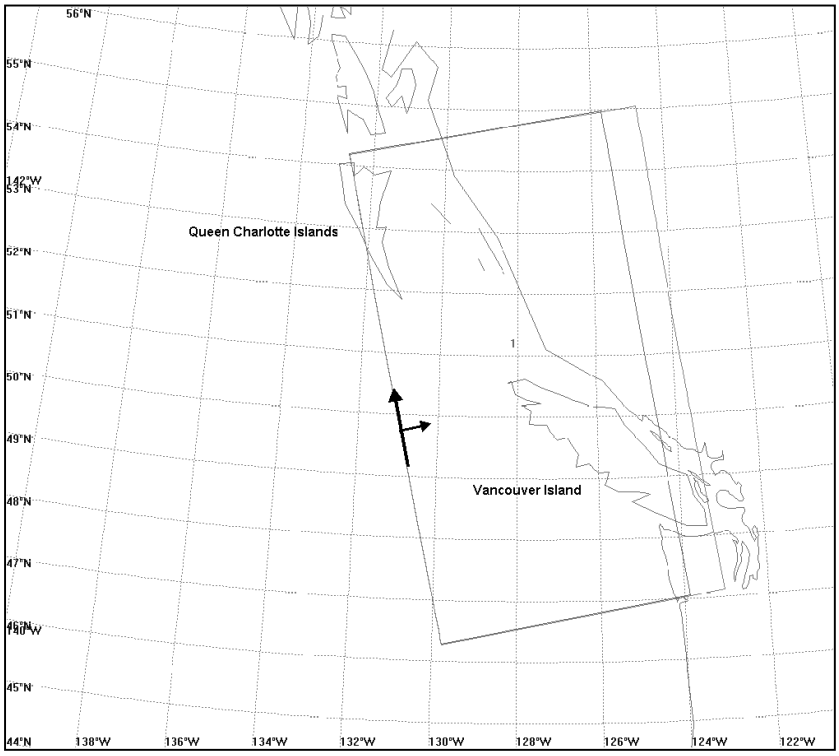

Figure 1. Map showing the study area off the West Coast of Canada. The box identifies the area that was imaged by RADARSAT on 29 July 1999. The radar look direction is to the right.

Table 1. SAR data acquisition and processing details; RADARSAT operated in the ScanSAR Wide B mode during ascending overpasses.

Date	Time (UTC)	Processed to Date
24 June 1999	02:39	
25 June 1999	02:08	
5 July 1999	02:16	
12 July 1999	02:12	√
18 July 1999	02:40	
29 July 1999	02:16	√
5 August 1999	02:12	
11 August 1999	02:39	
15 August 1999	02:20	
22 August 1999	02:16	
28 August 1999	02:43	
8 September 1999	02:20	√
15 September 1999	02:17	
21 September 1999	02:43	
29 September 1999	02:08	
2 October 1999	02:21	
9 October 1999	02:17	
16 October 1999	02:12	√

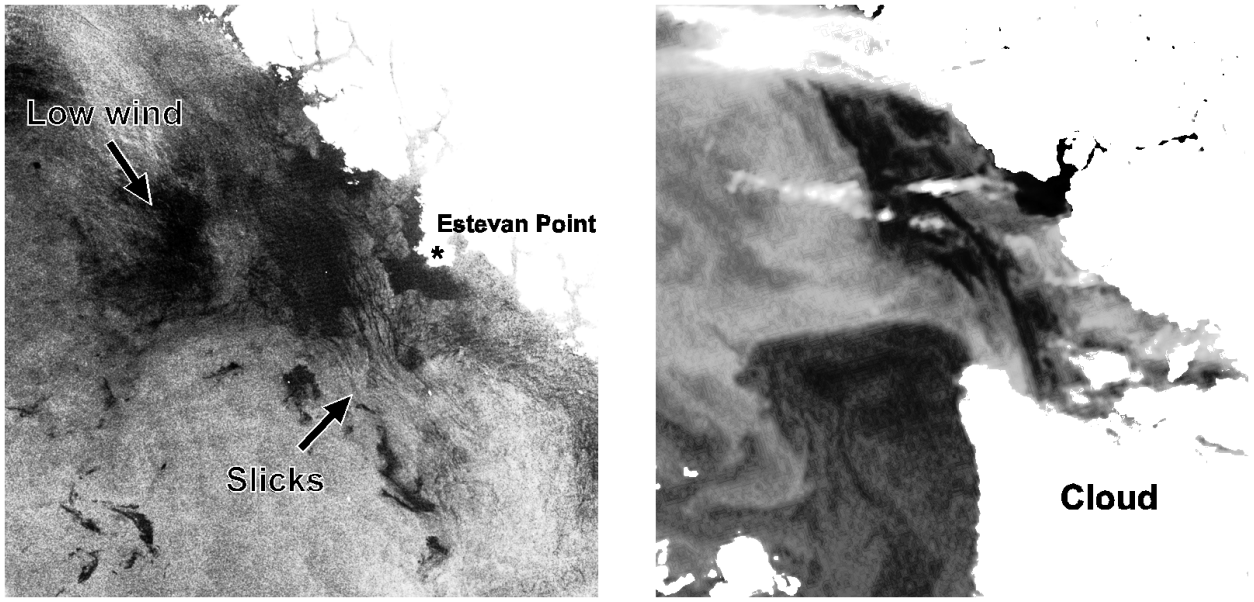

a b

Figure 2(a-b). Images showing coastal features off the west coast of Vancouver Island: (a) subset of RADARSAT ScanSAR Wide Beam image, 29 July 02:08 UTC (b) subset of first principal component produced from the thermal AVHRR channels, 30 July 01:24 UTC.

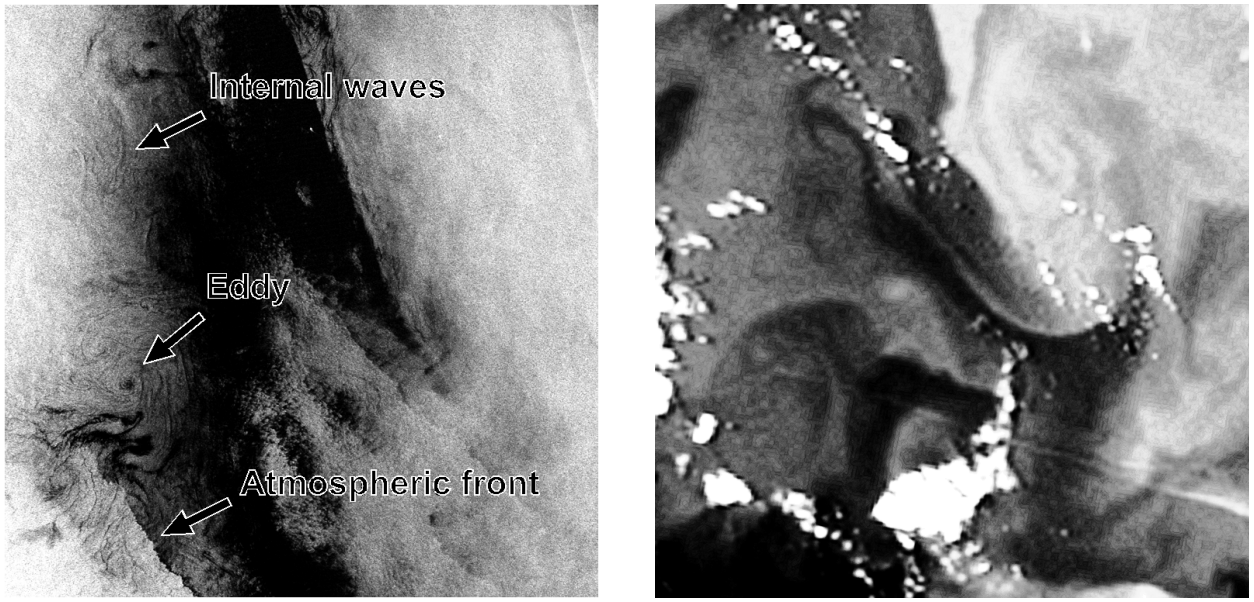

a b

Figure 3(a-b). Images showing coastal features off the west coast of Vancouver Island: (a) subset of RADARSAT ScanSAR Wide Beam image, 16 October 02:12 UTC (b) subset of first principal component produced from the thermal AVHRR channels, 15 October 16:13 UTC.

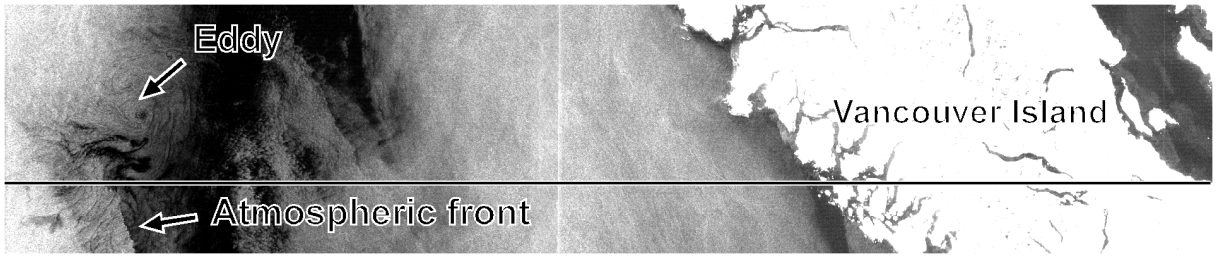

a

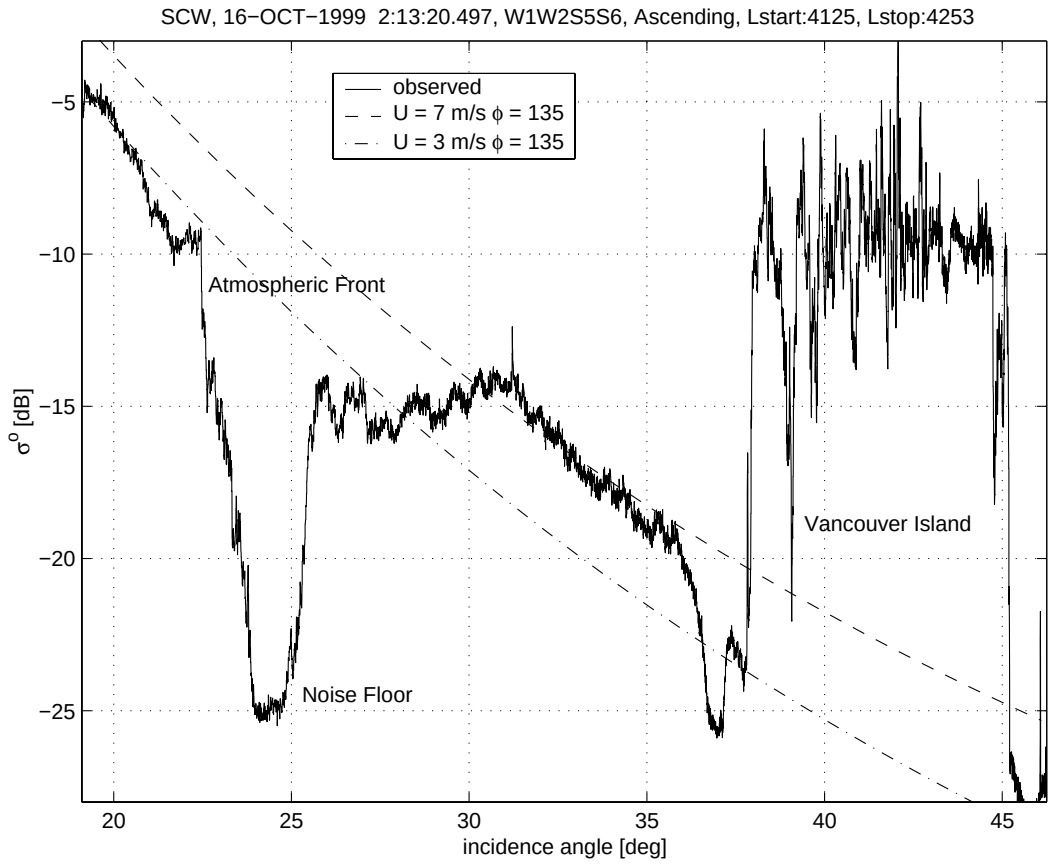

b

Figure 4(a-b). Backscatter transect through atmospheric front shown in ScanSAR image for 16 October 02:12 UTC: (a) SAR image with overlay showing the location of the transect (horizotal line) (b) observed and modelled Sigma nought values as a function of incidence angle; the modelling results correspond to wind speeds of 7 and 3 m s^{-1}.